



# A closed-form model for nonlinear spatial deflections of rectangular beams in intermediate range

Ruiyu Bai<sup>a,b</sup>, Shorya Awtar<sup>b</sup>, Guimin Chen<sup>a,c,\*</sup>

<sup>a</sup> School of Electro-Mechanical Engineering, Xidian University, Xi'an, Shaanxi 710071, China

<sup>b</sup> Precision Systems Design Lab, Mechanical Engineering, University of Michigan, 2350 Hayward Street, Ann Arbor, MI 48109, China

<sup>c</sup> State Key Laboratory for Manufacturing Systems Engineering and Shaanxi Key Lab of Intelligent Robots, Xi'an Jiaotong University, Xi'an, Shaanxi 710049, China

## ARTICLE INFO

### Keywords:

Rectangular beam  
Nonlinear spatial deflection  
Closed-form model

## ABSTRACT

Modeling the nonlinear load-displacement relations for flexible beams has been a key objective in compliant mechanisms research. There have been several practically useful methods for modeling planar deflections, but less work has been done in modeling spatial deflections. This work proposes the load-displacement relations for rectangular beams by solving the nonlinear governing differential equations of the beams using the power series method and then simplifying the solution by Taylor series expansion and truncation. The solution is validated to be accurate by comparing with two commercial finite element software packages, ANSYS and Abaqus. This comparison shows that this approach is capable of capturing the relevant geometric nonlinearities in the intermediate deflection range defined as 10% of the beam length. The load-displacement relation offers a useful and parameterized tool for understanding the constraint (i.e. stiffness and motion) behavior of rectangular cross-section beams and generating compliant mechanism designs with nonlinear kinetostatic behaviors.

## 1. Introduction

The aim of this work is to develop compact nonlinear load-displacement relations that capture the constraint characteristics of slender spatial beams of rectangular cross-section in the intermediate deflection range. The definition of the intermediate deflection range is as defined in Ref [1], i.e., the transverse deflections and rotations are limited to  $0.1L$  and  $0.1$  rad, respectively, where  $L$  is the beam length.

Modeling nonlinear deflections (both in the intermediate and large ranges) of flexible beams has been a key problem in compliant mechanisms (or flexure mechanisms) research [2], in that nonlinear deflections are essential for achieving various kinetostatic behaviors (e.g., multi-stable [3,4], constant-force [5–7] and statically balancing [8,9]) as well as understanding the constraint performances (namely stiffness and error motions) of compliant element and mechanism designs. There have been several practically useful methods for modeling planar deflections, for example, the planer beam constraint model (BCM) [1] and its derivatives [10,11] for deflections in the intermediate range, and the pseudo-rigid body models (PRBM) [12], the chain algorithm [2], the circular-arc method [13], the elliptical integral solutions [14], the Adomian decomposition method [15], the Gaussian-Chebyshev quadrature [16] and the chained beam constraint model [17] for large deflections.

The utilization of spatial beams in compliant mechanisms can bring about more diverse kinetostatic behaviors that could be useful in vari-

ous application including such as aerospace [18] and medical applications [19]. In contrast to planar beam models, less work has been done in deriving the end load-displacement relations for spatial deflections of beams. The formulation of governing differential equations for spatial beams can be found in multiple previous publications e.g. [20,21]. Numerical method such as the numerical integration method [22,23] and the nonlinear finite element methods (NLFEM) [24–26] can be employed to solve the governing equations. However, as noted in [27] these numerical methods offer little parametric design insight for designers and are usually used for validation. Several pseudo-rigid body models (PRBM) have been proposed to approximately model large spatial deflections, for example, Rasmussen et al. [28] proposed a 3D-PRBM (consisting of two rigid links joined by a spherical hinge that offer stiffness along three orthogonal directions) for rectangular beams subject to transverse tip forces. Chimento and Lusk [22] further developed this 3D PRBM for rectangular beams subject to arbitrary tip forces and Chase et al. [29] suggested to improve the modeling accuracy for spatial deflections of rectangular beams by serially connecting multiple 3D PRBMs. These PRBMs were developed to approximate the deflections of rectangular beams subject to pure tip forces and can yield large prediction errors when being used for general end loads. Also, by lumping all compliance to discrete joints, the PRBM does not capture the elastokinematic effect in slender planar and spatial beams [1,27].

\* Corresponding author.

E-mail address: [guimin.chen@xjtu.edu.cn](mailto:guimin.chen@xjtu.edu.cn) (G. Chen).

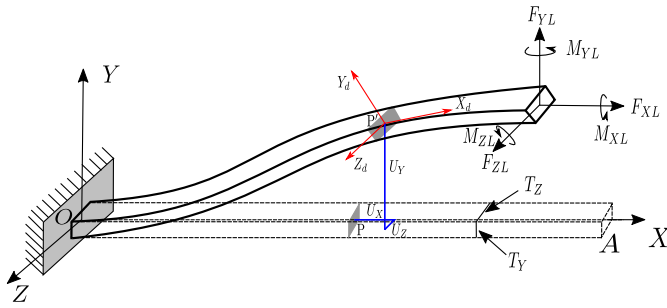


Fig. 1. Spatially deflected beam.

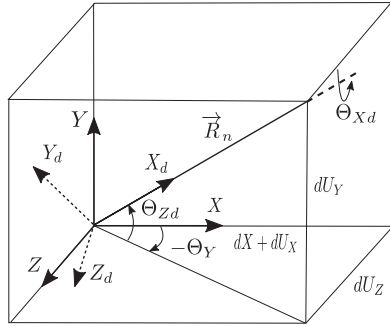


Fig. 2. Local coordinate system.

$$R = \begin{bmatrix} c(\Theta_Y)c(\Theta_{Z_d}) & s(\Theta_{Z_d}) & -c(\Theta_{Z_d})s(\Theta_Y) \\ s(\Theta_{X_d})s(\Theta_Y) - c(\Theta_{X_d})c(\Theta_Y)s(\Theta_{Z_d}) & c(\Theta_{X_d})c(\Theta_{Z_d}) & c(\Theta_Y)s(\Theta_{X_d}) + c(\Theta_{X_d})s(\Theta_Y)s(\Theta_{Z_d}) \\ c(\Theta_{X_d})s(\Theta_Y) + c(\Theta_Y)s(\Theta_{X_d})s(\Theta_{Z_d}) & -c(\Theta_{Z_d})s(\Theta_{X_d}) & c(\Theta_{X_d})c(\Theta_Y) - s(\Theta_{X_d})s(\Theta_Y)s(\Theta_{Z_d}) \end{bmatrix} \quad (1)$$

Hao et al. [30] proposed a composite method that employs two orthogonally arranged planar BCMs [1] together with a torsional equation to predict deflections of spatial beams in the intermediate range. However, it just can be used to model round or regular polygon cross-section beams. Sen and Awtar [27] developed and introduced a compact spatial BCM in the form of end load-displacement relations that capture key non-linearities in the spatial mechanics of the beam. But this final form of the model was derived only for spatial beams of bisymmetric cross-sections (e.g., square or circular cross-sections); the solutions to the governing equation for general beam cross-section proved to be mathematically too complex. This spatial BCM was further extended for modeling large spatial deflections for bisymmetric beams via a chain approach [31]. Nijenhuis et al. [32] developed an analytical model for the lateral stiffness of flexible strips, which is suitable for beams/plates whose width is at least one order of magnitude larger than the thickness where the displacement in the direction of width is far less than in the direction of thickness. But since this work assumed large beam width and small beam thickness, the displacement and rotation along the width direction are small (i.e. error motions) and do not contribute to the geometric non-linearities. Therefore, the results of this model are not relevant to more general rectangular cross-section beams with intermediate or large deflection in both bending directions. Generally speaking, there is a lack of a compact, parametric model that captures the nonlinear mechanics of a spatial beam with general rectangular cross-sections in terms of end load-displacement relations for even the intermediate deflection range.

The current work bridges this gap by solving the non-linear governing equations of a spatial slender beam, with a general rectangular cross-section, using the power series method to produce end-load displacement relations that capture relevant geometrical nonlinearities in the beam mechanics. This compact, parametric model represents the

spatial BCM for a general cross-section beam, which has previously not been reported. Although the model is limited to intermediate deflection range, it can be further extended for modeling large spatial deflections by employing a chain scheme, as has been successfully demonstrated previously in Refs. [31,33,34].

The rest of this paper is organized as follows. Sections 2 and 3 formulate the governing equations for rectangular beams in the intermediate deflection range by ensuring that the relevant geometric nonlinearities are included. The governing differential equations are then solved using the power series method for the load-displacement relations in Section 4. The accuracy of the model is validated using two commercial finite element software packages (ANSYS and Abaqus) in Section 5. Concluding remarks are included in Section 6.

## 2. Spatial deflection of the flexible beam

As shown in Fig. 1, a cantilever beam is deflected due to a general load exerted on its free end. Following the same notation as Sen and Awtar [27], a global coordinates frame XYZ is established at its fixed end O, with the X-, Y- and Z-axes are in the direction of the centroidal axis, the thickness direction and the width direction of the undeflected beam, respectively. An arbitrary point P (X, 0, 0) on the centroidal axis of the undeflected beam moves to P' (X + U<sub>X</sub>, U<sub>Y</sub>, U<sub>Z</sub>) after deflection. The Tait-Bryan angles (Θ<sub>X<sub>d</sub></sub>, Θ<sub>Y</sub> and Θ<sub>Z<sub>d</sub></sub> as shown in Fig. 2) are used to represent the orientation of the cross section. A local coordinate frame X<sub>d</sub>Y<sub>d</sub>Z<sub>d</sub> is established at P' with the X<sub>d</sub>-axis along the tangent of the deformed centroidal axis at this point, and the Y<sub>d</sub>- and Z<sub>d</sub>-axes are parallel to the Y- and Z-axes when the beam is undeflected, respectively. The transformation matrix from frame XYZ to frame X<sub>d</sub>Y<sub>d</sub>Z<sub>d</sub> can be expressed by the Tait-Bryan angles as

in which  $c(\Theta) \triangleq \cos(\Theta)$  and  $s(\Theta) = \sin(\Theta)$ .

Similar to Ref [27], it is assumed that translation and rotation of the beam tip are less than 0.1L and 0.1 rad, which means that the values of U'<sub>X</sub>, U'<sub>Y</sub> and U'<sub>Z</sub> are of the orders of 10<sup>-2</sup>, 10<sup>-1</sup> and 10<sup>-1</sup> of the length of the beam, respectively, and we have

$$\begin{cases} \Theta_Y \approx -U'_Z \\ \Theta_{Z_d} \approx U'_Y \end{cases}$$

The curvatures along the direction of X<sub>d</sub>, Y<sub>d</sub> and Z<sub>d</sub> (denoted as κ<sub>X<sub>d</sub></sub>, κ<sub>Y<sub>d</sub></sub> and κ<sub>Z<sub>d</sub></sub>, respectively) of the deflected beam can be given as [21,27,32] as

$$\begin{cases} \kappa_{X_d} \approx \Theta'_{X_d} + \Theta'_Y \Theta_{Z_d} = \Theta'_{X_d} - U''_Z U'_Y \\ \kappa_{Y_d} \approx \Theta'_Y + \Theta_{X_d} \Theta'_{Z_d} = -U''_Z + \Theta_{X_d} U''_Y \\ \kappa_{Z_d} \approx \Theta'_{Z_d} - \Theta_{X_d} \Theta'_Y = U''_Y + \Theta_{X_d} U''_Z \end{cases} \quad (2)$$

and the normal strain along the X<sub>d</sub>-direction (denoted as ε<sub>XX</sub>) as

$$\epsilon_{XX} = U'_X + \frac{1}{2}U'^2_Y + \frac{1}{2}U'^2_Z - T_Y \kappa_{Z_d} + T_Z \kappa_{Y_d} + \frac{1}{2}\kappa^2_{X_d}(T^2_Y + T^2_Z) \quad (3)$$

Because the beam we interested in is slender beam, the shear deflections caused by transverse loads (F<sub>Y<sub>L</sub></sub> and F<sub>Z<sub>L</sub></sub>) are ignored. But the shear strain results from torsional moment give rise to the warping of the plane and makes great influence to torsional deflection for slender beams [21]. In practice, the torsional deflection including cross-sectional warping can be captured by using an effective torsional constant and for rectangular beams, the exact torsional constant is given as [20]

$$J = \frac{T_Y T_Z^3}{3} \left[ 1 - \frac{192 T_Z}{\pi^5 T_Y} \sum_{n=1,3,5,\dots}^{\infty} \frac{\tanh(n\pi \frac{T_Y}{2T_Z})}{n^5} \right] \quad (4)$$

The equation involves summing up of an infinite series and requires T<sub>Y</sub> ≥ T<sub>Z</sub>. Therefore, we use the torsional constant that is independent of

**Table 1**  
The six load case.

Case	$F_{XL}$ (N)	$F_{YL}$ (N)	$F_{ZL}$ (N)	$M_{XL}$ (N·m)	$M_{YL}$ (N·m)	$M_{ZL}$ (N·m)
1	3	-1, -0.9, -0.8, ..., 1	0	0.07	0	0
2	3	0	0	0.07	0	-0.07, -0.063, -0.056, ..., 0.07
3	-3	0	-2.5, -2.25, -2, ..., 2.5	0.07	0	0
4	-3	0	0	-0.07	-0.5, -0.45, -0.4, ..., 0.5	0
5	-3, -2.7, -2.4, ..., 3	0.05	2.5	0.07	0.5	0.05
6	3	0.05	2.5	-0.08, -0.072, -0.064, ..., 0.08	0.5	0.05

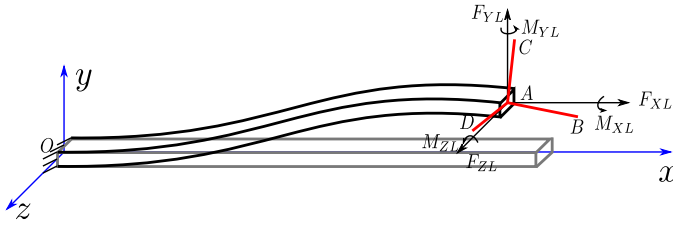


**Fig. 3.** A structure consisting of three mutually perpendicular beams is introduced in NLFEM.

the aspect ratio proposed in Ref [35]:

$$J = \frac{2T_Y^3 T_Z^3}{7T_Y^2 + 7T_Z^2} f(\eta) \quad (5)$$

where  $\eta$  is the aspect ratio (i.e. the ratio between  $T_Y$  and  $T_Z$ ) and

$$f(\eta) = \frac{1.167\eta^5 + 29.49\eta^4 + 30.9\eta^3 + 100.9\eta^2 + 30.38\eta + 29.41}{\eta^5 + 25.91\eta^4 + 41.58\eta^3 + 90.43\eta^2 + 41.74\eta + 25.21} \quad (6)$$

As the curvature and the strain are expressed with respect to the local coordinate frame, the moments as this point should be given with respect to this frame as well. The moments can be expressed by the free-end loads ( $F_{XL}$ ,  $F_{YL}$ ,  $F_{ZL}$ ,  $M_{XL}$ ,  $M_{YL}$  and  $M_{ZL}$  as shown in Fig. 1) as follows:

$$\begin{cases} M_X = M_{XL} + F_{ZL}(U_{YL} - U_Y) - F_{YL}(U_{ZL} - U_Z) \\ M_Y = M_{YL} - F_{ZL}(L - X) + F_{XL}(U_{ZL} - U_Z) \\ M_Z = M_{ZL} + F_{YL}(L - X) - F_{XL}(U_{YL} - U_Y) \end{cases} \quad (7)$$

Using the transformation in Eq. (1) and truncating the higher-order terms, the moments with respect to the local coordinate frame can be derived as

$$\begin{cases} M_{Xd} = M_X + U'_Y M_Y + U'_Z M_Z \\ M_{Yd} = M_Y - U'_Y M_X + \Theta_{Xd} M_Z \\ M_{Zd} = M_Z - U'_Z M_X - \Theta_{Xd} M_Y \end{cases} \quad (8)$$

### 3. Governing differential equations for spatial beams

For a beam of rectangular cross-section deflected by a general end load (comprised of  $F_{XL}$ ,  $F_{YL}$ ,  $F_{ZL}$ ,  $M_{Xd}$ ,  $M_{Yd}$  and  $M_{Zd}$ ), the constitutive formulas are given in reference [32] as (linear elastic material is assumed):

$$\begin{bmatrix} F_{XL} \\ F_{YL} \\ F_{ZL} \\ M_{Xd} \\ M_{Yd} \\ M_{Zd} \end{bmatrix} = \begin{bmatrix} EA\gamma_{Xd} \\ GAk_Y\gamma_{Yd} \\ GAk_Z\gamma_{Zd} \\ GJ\kappa_{Xd} \\ EI_Y\kappa_{Yd} \\ EI_Z\kappa_{Zd} \end{bmatrix} \quad (9)$$

where  $E$  is the Young's modulus,  $G$  is the shear modulus,  $k_Y$  and  $k_Z$  are the shear correction factors.  $\gamma_{Xd}$ ,  $\gamma_{Yd}$  and  $\gamma_{Zd}$  are the strain components in the  $X$ -,  $Y$ - and  $Z$ - axes, respectively.  $I_Y$  and  $I_Z$  are the moments of

inertia in the directions of thickness and width, respectively, and  $J$  is the torsional constant.

Because we neglect the shear deflections produced by  $F_{YL}$  and  $F_{ZL}$ , the second and third formulas are dropped thus only four formulas remain. The first formula represents the arc-length of the beam equals the original length  $L$  plus the extension/contraction by the axial force  $F_{XL}$ . Accordingly,  $F_{XL}$  is expressed as

$$\begin{aligned} F_{XL} &= E \iint_A \epsilon_{XX} dA \\ &= E \int_{-T_Z/2}^{T_Z/2} \int_{-T_Y/2}^{T_Y/2} (U'_X + \frac{1}{2}U'^2_Y + \frac{1}{2}U'^2_Z - T_Y\kappa_{Zd} + T_Z\kappa_{Yd} \\ &\quad + \frac{1}{2}\kappa^2_{Xd}(T^2_Y + T^2_Z)) dY dZ \\ &= EA(U'_X + \frac{1}{2}U'^2_Y + \frac{1}{2}U'^2_Z) + \frac{E(I_Y + I_Z)}{2} \kappa^2_{Xd} \\ &\approx EA(U'_X + \frac{1}{2}U'^2_Y + \frac{1}{2}U'^2_Z) \end{aligned} \quad (10)$$

where  $\frac{E(I_Y + I_Z)}{2} \kappa^2_{Xd}$  represents the nonlinearity due to trapeze effect which is small enough to neglect for the spatial deflections [21]. Besides, we have derived the  $M_{Xd}$ ,  $M_{Yd}$  and  $M_{Zd}$  in Eq. (8) and  $\kappa_{Xd}$ ,  $\kappa_{Yd}$  and  $\kappa_{Zd}$  in Eq. (2), respectively. Accordingly, governing differential equations of the spatial deformed beam are expressed as

$$\begin{cases} \Theta'_{Xd} - U''_Z U'_Y = \frac{M_X + U'_Y M_Y + U'_Z M_Z}{GJ} \\ -U''_Z + \Theta_{Xd} U''_Y = \frac{M_Y - U'_Y M_X + \Theta_{Xd} M_Z}{EI_Y} \\ U''_Y + \Theta_{Xd} U''_Z = \frac{M_Z - U'_Z M_X - \Theta_{Xd} M_Y}{EI_Z} \\ F_{XL} = EA(U'_X + \frac{1}{2}U'^2_Y + \frac{1}{2}U'^2_Z) \end{cases} \quad (11)$$

While the beam is fixed at point  $O$ , the geometric boundary conditions can be expressed as

$$\begin{cases} U_{X0} = 0 & U_{Y0} = 0 & U_{Z0} = 0 \\ \Theta_{Xd0} = 0 & U'_{Y0} = 0 & U'_{Z0} = 0 \end{cases} \quad (12)$$

A normalization scheme similar to Ref [1] is used, in which the normalized parameters of the loads and deflections are defined as

$$\begin{cases} f_{x1} = \frac{F_{XL} L^2}{EI_Z} & f_{y1} = \frac{F_{YL} L^2}{EI_Z} & f_{z1} = \frac{F_{ZL} L^2}{EI_Z} \\ m_{x1} = \frac{M_{XL} L}{EI_Z} & m_{y1} = \frac{M_{YL} L}{EI_Z} & m_{z1} = \frac{M_{ZL} L}{EI_Z} \\ u_y = \frac{U_Y}{L} & u_z = \frac{U_Z}{L} & \theta_{Xd} = \Theta_{Xd} & x = \frac{X}{L} \end{cases} \quad (13)$$

By substituting Eq. (13) into Eq. (11), the beam governing differential equations can be rewritten as

$$\begin{cases} \theta'_{xd} - u''_z u'_y = \frac{m_x + m_y u'_y + m_z u'_z}{k_{44}} \\ \theta_{xd} u''_y - u''_z = \alpha(m_y - m_x u'_y + m_z \theta_{xd}) \\ u''_y + \theta_{xd} u''_z = m_z - m_x u'_z - m_y \theta_{xd} \\ \frac{f_{x1}}{k_{33}} = u'_x + \frac{1}{2} u'^2_y + \frac{1}{2} u'^2_z \end{cases} \quad (14)$$

where  $\alpha = \frac{I_Z}{I_Y}$ ,  $k_{33} = \frac{L^2 A}{I_Z}$  and  $k_{44} = \frac{GJ}{EI_Z}$ . The normalized moments  $m_x$ ,  $m_y$  and  $m_z$  are derived by combining Eqs. (7), (8) and (13):

$$\begin{cases} m_x = m_{x1} + f_{z1}(u_{y1} - u_y) - f_{y1}(u_{z1} - u_z) = m_{x0} - f_{z1}u_y + f_{y1}u_z \\ m_y = m_{y1} - f_{z1}(1 - x) + f_{x1}(u_{z1} - u_z) = m_{y0} + f_{z1}x - f_{x1}u_z \\ m_z = m_{z1} + f_{y1}(1 - x) - f_{x1}(u_{y1} - u_y) = m_{z0} - f_{y1}x + f_{x1}u_y \end{cases} \quad (15)$$

where the subscripts "0" and "1" in the load parameters indicate that they are measured at the fixed end and the free end of the beam, re-

spectively. The use of the moments at the fixed end makes the end load-displacement expressions more compact as will be shown in the next section. Especially, for beams of bisymmetrical cross-sections (i.e.  $\alpha = 1$ ), Eq. (14) should be similar to the governing equations in [27]. However, there are two key differences in these two sets of governing equations. One, the 1st and 4th equations in Eq. (14) neglect the coupling between axial and torsion directions, which is shown as the trapeze effect in reference [27] and makes very small contribution (<1% errors) to the results when the beam subject to spatial deflections. Another difference is that the 2nd and 3rd equations in Eq. (14), which represent the bending in XY and XZ planes, involve terms of twisting angles that shows the coupling between bending and torsion. These terms were dropped in bisymmetric SBCM without loss of precision [27], but they cannot be neglected for rectangular beam. Also, these governing equations are in agreement with those in Nijenhuis's paper [32] and Hodges's paper [25], both of which provide governing equations for a general cross-section beam and not simply a bisymmetric cross-section beam. It should be noted that Eq. (14) are nonconstant coefficient differential equations and cannot be solved directly. To solve linear differential equations with variable coefficients, the power series method [36] has been used previously in the modeling

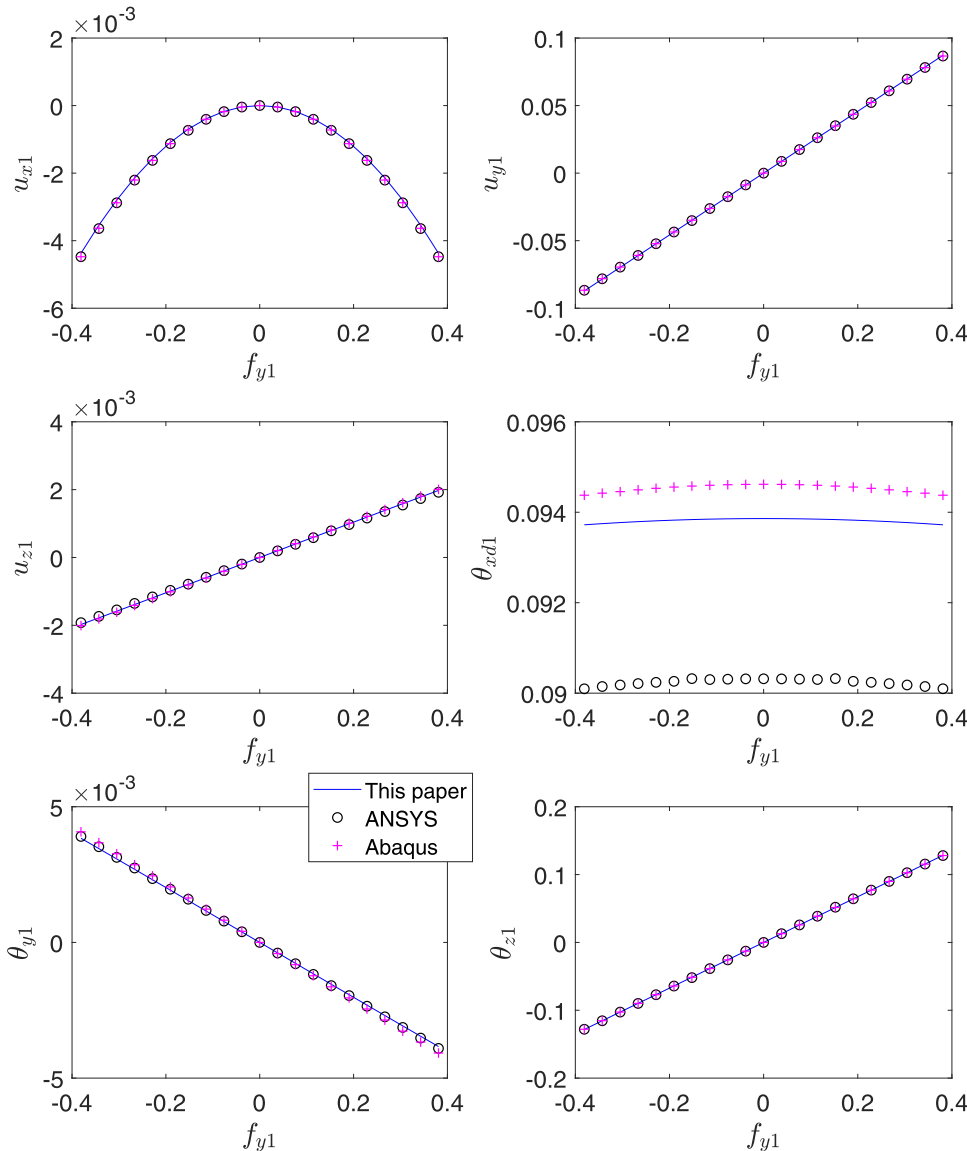


Fig. 4. Deflections vs.  $f_y$  (load case 1).

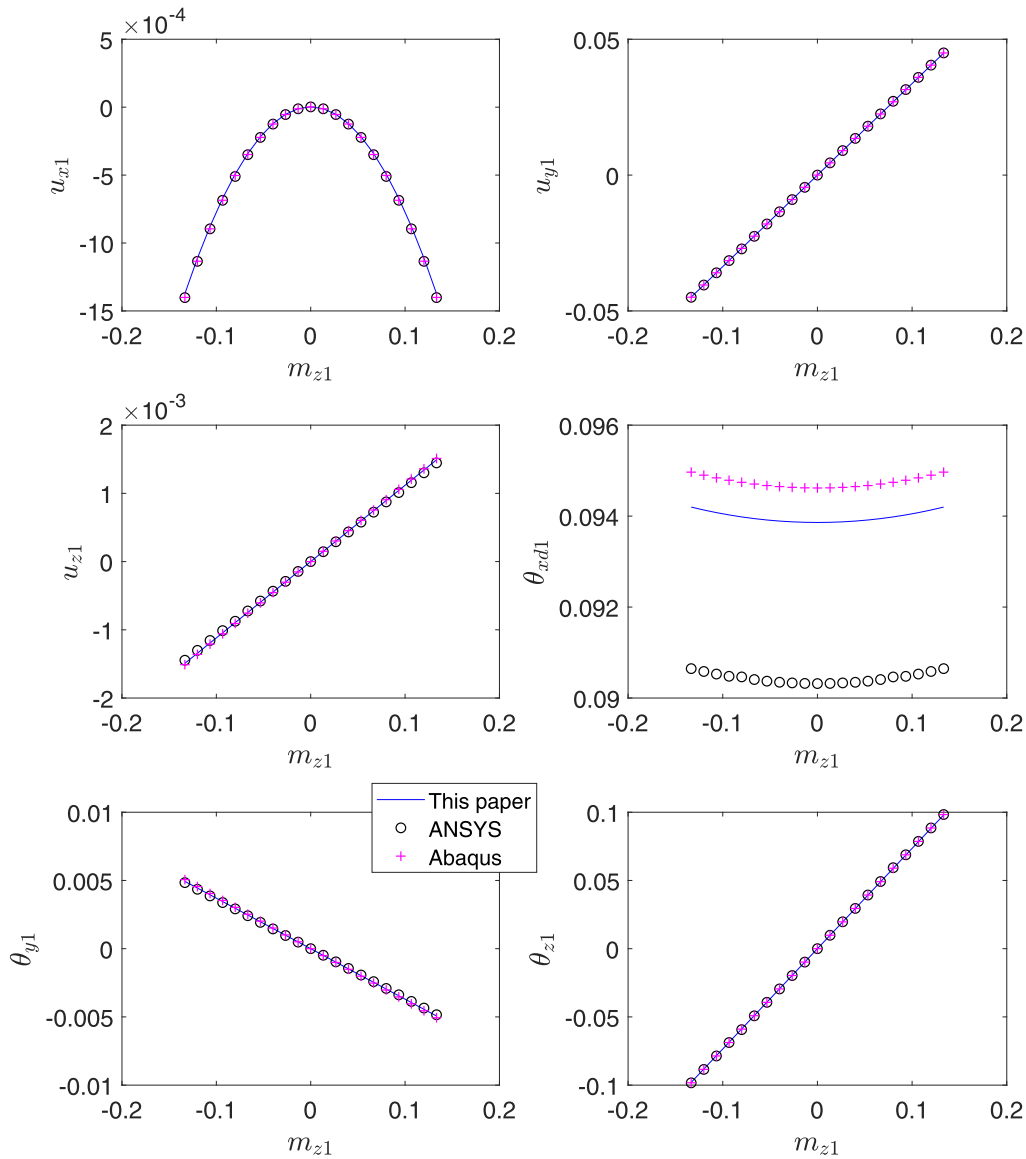


Fig. 5. Deflections vs.  $m_z$  (load case 2).

of planar beams [1]. The same approach will be employed here as well.

#### 4. Solution

To solve a differential equation, the power series method assumes that the solution can be expressed as a power series with unknown coefficients, then substitutes the power series into the differential equation to find the recurrence relations for the coefficients.

By following the power series method, we express the deflections as

$$\begin{cases} u_x = \sum_{n=0}^{\infty} a_n^x x^n; \\ \theta_{xd} = \sum_{n=0}^{\infty} a_n^{xd} x^n \\ u_y = \sum_{n=0}^{\infty} a_n^y x^n; \\ u_z = \sum_{n=0}^{\infty} a_n^z x^n; \end{cases} \quad (16)$$

Differentiating Eq. (16) yields the following derivatives:

$$\begin{cases} u'_x = \sum_{n=1}^{\infty} n a_n^x x^{n-1} \\ \theta'_{xd} = \sum_{n=1}^{\infty} n a_n^{xd} x^{n-1} \\ u'_y = \sum_{n=1}^{\infty} n a_n^y x^{n-1} \\ u''_y = \sum_{n=2}^{\infty} n(n-1) a_n^y x^{n-2} \\ u'_z = \sum_{n=1}^{\infty} n a_n^z x^{n-1} \\ u''_z = \sum_{n=2}^{\infty} n(n-1) a_n^z x^{n-2} \end{cases} \quad (17)$$

Substituting Eqs. (16) and (17) into the governing differential equations of Eq. (14) and applying the following geometric boundary conditions

$$\begin{cases} u_{x0} = 0; & u_{y0} = 0; & u_{z0} = 0 \\ \theta_{xd0} = 0; & u'_{y0} = 0; & u'_{z0} = 0 \end{cases} \quad (18)$$

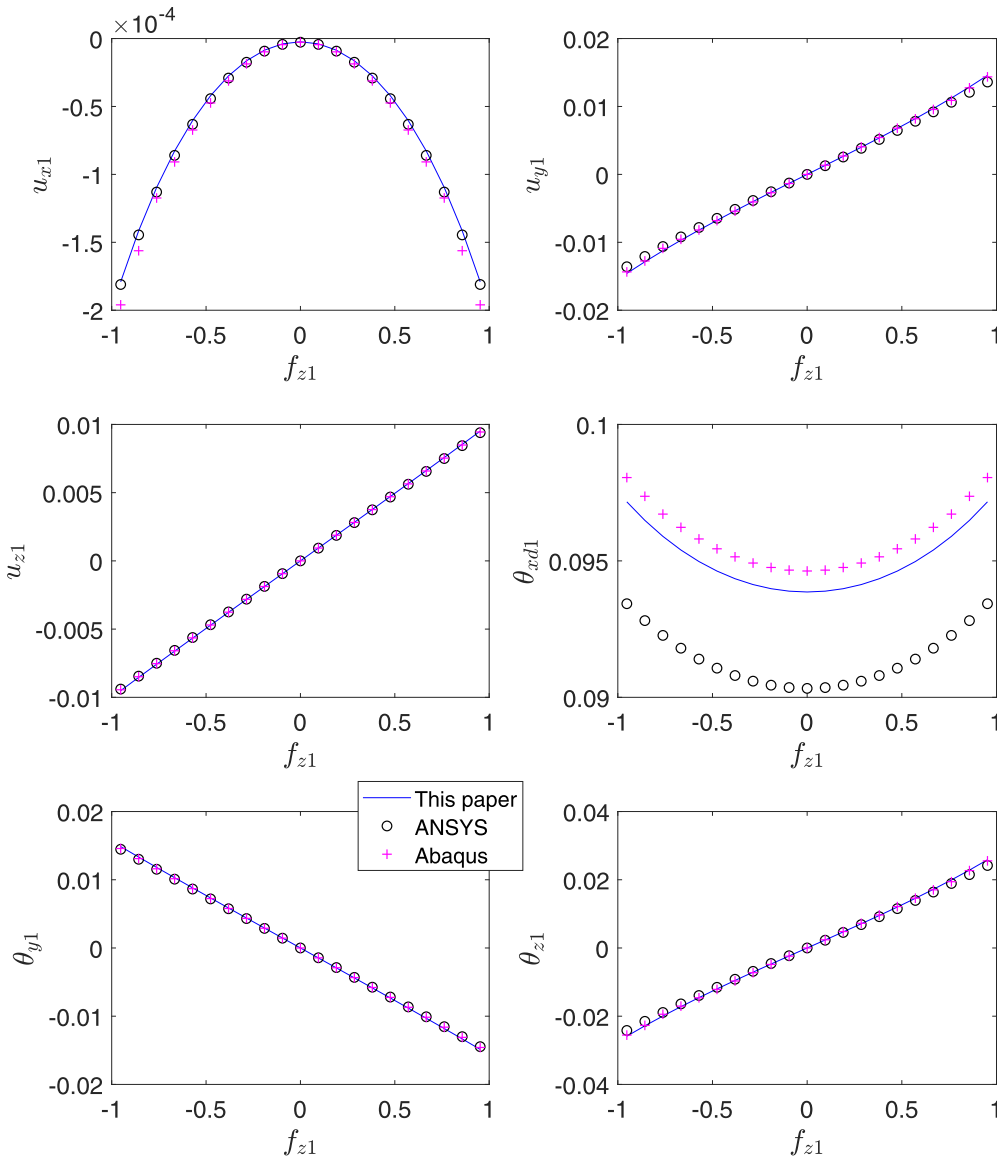


Fig. 6. Deflections vs.  $f_z$  (load case 3).

yield the recurrence relations, which are further used to solve for the coefficients of the power series  $a_n^x$ ,  $a_n^y$ ,  $a_n^z$  and  $a_n^{xd}$ . However, since the recurrence relations are hard to derive by hand, we turn to use the software "Maple" to get the power series solution by using the command "dsolve" and choosing the option as "series" (only the first eight coefficients in each power series are solved considering that the eighth and higher power terms become insignificant).

The coefficients are functions of loads and cross-sectional parameters. When the beam is deflected in the intermediate range, the normalized transverse loads are in  $[-1, 1]$  range. Since the coefficients of the 3rd and higher order terms of loads are much smaller than the 1st order terms, these terms can be neglected directly. The 8th and higher power terms of  $x$  in Eq. (16) do not contain the 1st and 2nd order terms of transverse loads, which means these terms are much smaller than the 7th and lower power terms, thus are dropped. By taking the Taylor series expansions of the coefficients with respect to  $f_{x1}$  and  $m_{x0}$  and dropping the third and higher power terms (they are insignificant for transverse deflections and rotations in the intermediate range), the following deflection-load relations can be

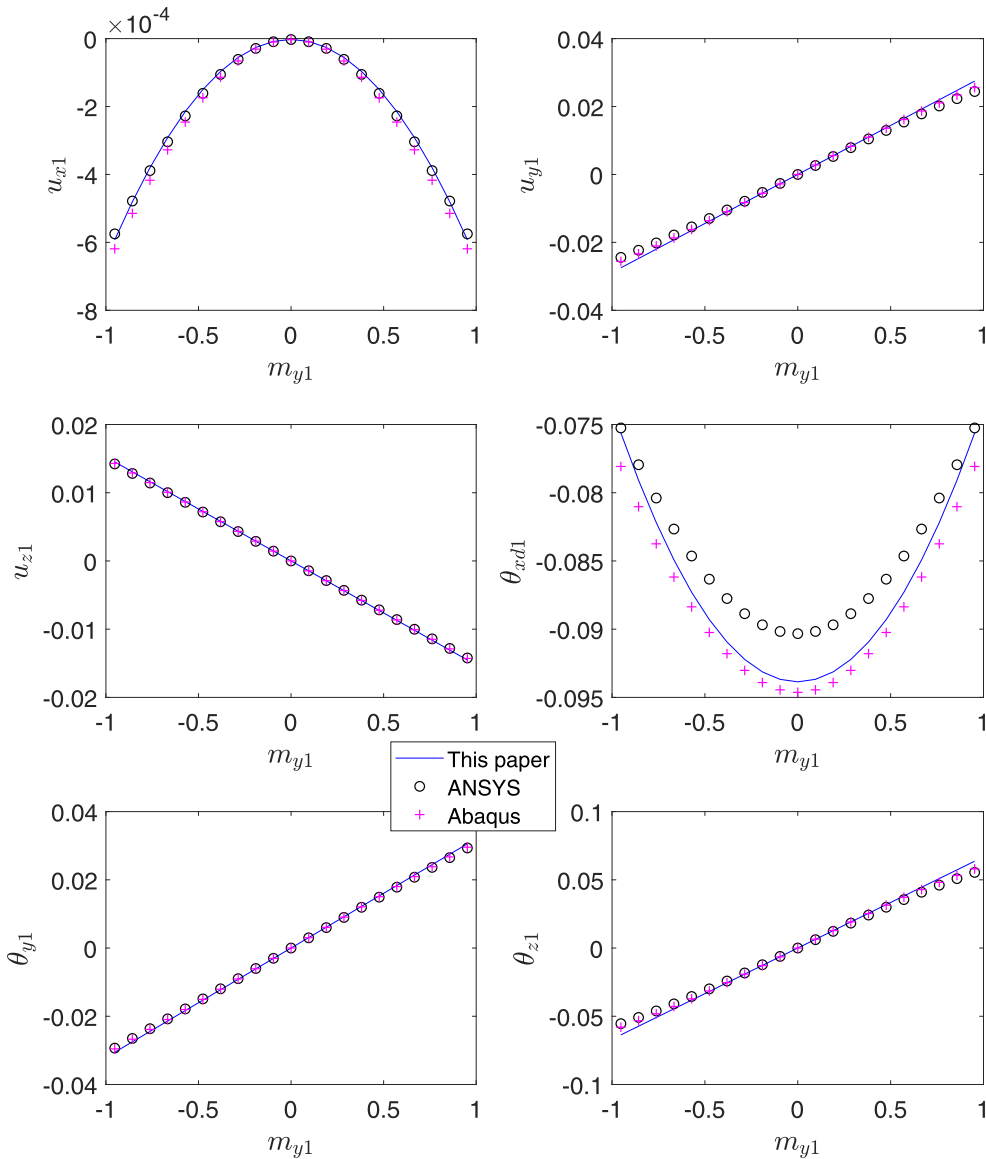
obtained:

$$\begin{bmatrix} u_{y1} \\ u'_{y1} \\ u_{z1} \\ -u'_{z1} \end{bmatrix} = (C_1 + f_{x1}C_2 + m_{x0}C_3 + f_{x1}^2C_4 + f_{x1}m_{x0}C_5 + m_{x0}^2C_6) \begin{bmatrix} f_{y1} \\ m_{z0} \\ f_{z1} \\ m_{y0} \end{bmatrix} \quad (19)$$

$$\theta_{xd1} = \frac{m_{x0}}{k_{44}} + [f_{y1} \quad m_{z0} \quad f_{z1} \quad m_{y0}](C_{t1} + f_{x1}C_{t2} + m_{x0}C_{t3}) \begin{bmatrix} f_{y1} \\ m_{z0} \\ f_{z1} \\ m_{y0} \end{bmatrix} \quad (20)$$

$$u_{x1} = \frac{f_{x1}}{k_{33}} + [f_{y1} \quad m_{z0} \quad f_{z1} \quad m_{y0}](C_{x1} + f_{x1}C_{x2} + m_{x0}C_{x3}) \begin{bmatrix} f_{y1} \\ m_{z0} \\ f_{z1} \\ m_{y0} \end{bmatrix} \quad (21)$$

Fig. 7. Deflections vs.  $m_y$  (load case 4).



in which  $C_i$  ( $i = 1, 2, \dots, 6$ ),  $C_{xj}$  and  $C_{ij}$  ( $j = 1, 2, 3$ ) represent various aspects of compliance in the beam. By simplifying the remaining coefficients,  $C_{iv}$ ,  $C_{xj}$  and  $C_{ij}$  are derived as

$$C_1 = \frac{1}{6} \begin{bmatrix} -1 & 3 & 0 & 0 \\ -3 & 6 & 0 & 0 \\ 0 & 0 & -\alpha & -3\alpha \\ 0 & 0 & 3\alpha & 6\alpha \end{bmatrix}$$

$$C_2 = \frac{1}{120} \begin{bmatrix} -1 & 5 & 0 & 0 \\ -5 & 20 & 0 & 0 \\ 0 & 0 & -\alpha^2 & -5\alpha^2 \\ 0 & 0 & 5\alpha^2 & 20\alpha^2 \end{bmatrix}$$

$$C_3 = \begin{bmatrix} 0 & 0 & \frac{k_{44}\alpha + 2\beta}{24k_{44}} & \frac{k_{44}\alpha + \beta}{6k_{44}} \\ 0 & 0 & \frac{k_{44} + 2\beta}{6k_{44}} & \frac{k_{44}\alpha + \beta}{2k_{44}} \\ -\frac{k_{44} - 2\beta}{24k_{44}} & \frac{k_{44}\alpha - \beta}{6k_{44}} & 0 & 0 \\ \frac{k_{44} - 2\beta}{6k_{44}} & -\frac{k_{44}\alpha - \beta}{2k_{44}} & 0 & 0 \end{bmatrix}$$

$$C_4 = \frac{1}{5040} \begin{bmatrix} -1 & 7 & 0 & 0 \\ -7 & 42 & 0 & 0 \\ 0 & 0 & -\alpha^3 & -7\alpha^3 \\ 0 & 0 & 7\alpha^3 & 42\alpha^3 \end{bmatrix}$$

$$C_5 = \begin{bmatrix} 0 & 0 & \frac{k_{44}(\alpha^2 + \alpha) + 2\beta(2\alpha + 1)}{720k_{44}} & \frac{k_{44}(\alpha^2 + \alpha) + \beta(3\alpha + 1)}{120k_{44}} \\ 0 & 0 & \frac{k_{44}(\alpha^2 + \alpha) + 2\beta(2\alpha + 1)}{120k_{44}} & \frac{k_{44}(\alpha^2 + \alpha) + \beta(3\alpha + 1)}{24k_{44}} \\ -\frac{k_{44}(\alpha^2 + \alpha) + 2k_{44} - 6\beta}{720k_{44}} & \frac{k_{44}(\alpha^2 + \alpha) - \beta(\alpha + 3)}{120k_{44}} & 0 & 0 \\ \frac{k_{44}(\alpha^2 + \alpha) + 2k_{44} - 6\beta}{120k_{44}} & -\frac{k_{44}(\alpha^2 + \alpha) - \beta(\alpha + 3)}{24k_{44}} & 0 & 0 \end{bmatrix}$$

$$C_6 = \begin{bmatrix} \frac{(k_{44}^2 + k_{44})\alpha + 2k_{44} - 6\beta}{120k_{44}^2} & -\frac{(k_{44}^2 + k_{44})\alpha + 2k_{44} - 6\beta}{24k_{44}^2} & 0 & 0 \\ \frac{(k_{44}^2 + k_{44})\alpha + 2k_{44} - 6\beta}{24k_{44}^2} & -\frac{(k_{44}^2 + k_{44})\alpha + 2k_{44} - 6\beta}{6k_{44}^2} & 0 & 0 \\ 0 & 0 & \frac{(k_{44}^2 + 2k_{44})\alpha^2 + k_{44} + 6\beta}{120k_{44}^2} & \frac{(k_{44}^2 + k_{44})\alpha^2 + k_{44} + 2\beta}{24k_{44}^2} \\ 0 & 0 & -\frac{(k_{44}^2 + 2k_{44})\alpha^2 + k_{44} + 6\beta}{24k_{44}^2} & -\frac{(k_{44}^2 + k_{44})\alpha^2 + k_{44} + 2\beta}{6k_{44}^2} \end{bmatrix}$$

$$C_{r1} = \begin{bmatrix} 0 & 0 & \frac{3k_{44}\alpha + 2\beta}{48k_{44}} & \frac{k_{44}\alpha + \beta}{12k_{44}} \\ 0 & 0 & -\frac{2k_{44} + \beta}{12k_{44}} & \frac{k_{44}\alpha + \beta}{4} \\ \frac{3k_{44}\alpha + 2\beta}{48k_{44}} & -\frac{2k_{44} + \beta}{12k_{44}} & 0 & 0 \\ \frac{k_{44}\alpha + \beta}{12k_{44}} & \frac{k_{44}\alpha + \beta}{4} & 0 & 0 \end{bmatrix}$$

$$C_{r2} = \begin{bmatrix} 0 & 0 & \frac{10k_{44}^2\alpha^2 + 5k_{44}\alpha + 4\alpha^2 - 4}{1440k_{44}} & \frac{6k_{44}\alpha^2 + k_{44}\alpha + \beta(3\alpha + 1)}{240k_{44}} \\ 0 & 0 & \frac{4k_{44}\alpha^2 + 4k_{44}\alpha + \beta(\alpha + 3)}{240k_{44}} & -\frac{3k_{44}\alpha^2 + k_{44}\alpha + \alpha^2 - 1}{48k_{44}} \\ \frac{10k_{44}^2\alpha^2 + 5k_{44}\alpha + 4\alpha^2 - 4}{1440k_{44}} & -\frac{4k_{44}\alpha^2 + 4k_{44}\alpha + \beta(\alpha + 3)}{240k_{44}} & 0 & 0 \\ \frac{6k_{44}\alpha^2 + k_{44}\alpha + \beta(3\alpha + 1)}{240k_{44}} & -\frac{3k_{44}\alpha^2 + k_{44}\alpha + \alpha^2 - 1}{48k_{44}} & 0 & 0 \end{bmatrix}$$

$$C_{i3} = \begin{bmatrix} \frac{2k_{44}^2 - 3k_{44}\alpha + 4k_{44} - 2\beta}{40k_{44}^2} & \frac{6k_{44}^2\alpha - 6k_{44}\alpha + 9k_{44} - 4\beta}{48k_{44}^2} & 0 & 0 \\ \frac{6k_{44}^2\alpha - 6k_{44}\alpha + 9k_{44} - 4\beta}{48k_{44}^2} & \frac{2k_{44}^2\alpha - k_{44}\alpha + 2k_{44} - \beta}{6k_{44}^2} & 0 & 0 \\ 0 & 0 & -\frac{4k_{44}^2\alpha^2 + 8k_{44}\alpha^2 - 11k_{44}\alpha - 6\beta}{120k_{44}^2} & -\frac{4k_{44}^2\alpha^2 + 5k_{44}\alpha^2 - 8k_{44}\alpha - 4\beta}{48k_{44}^2} \\ 0 & 0 & \frac{4k_{44}^2\alpha^2 + 5k_{44}\alpha^2 - 8k_{44}\alpha - 4\beta}{48k_{44}^2} & -\frac{k_{44}^2\alpha^2 + k_{44}\alpha^2 - 2k_{44}\alpha - \beta}{6k_{44}^2} \end{bmatrix}$$

$$C_{x1} = \begin{bmatrix} -\frac{1}{40} & -\frac{1}{16} & 0 & 0 \\ \frac{1}{16} & -\frac{1}{6} & 0 & 0 \\ 0 & 0 & -\frac{\alpha^2}{40} & -\frac{\alpha^2}{16} \\ 0 & 0 & -\frac{\alpha^2}{16} & -\frac{\alpha^2}{6} \end{bmatrix}$$

$$C_{x2} = -\frac{1}{1680} \begin{bmatrix} 5 & -\frac{35}{2} & 0 & 0 \\ -\frac{35}{2} & 56 & 0 & 0 \\ 0 & 0 & 5\alpha^2 & \frac{35}{2}\alpha^3 \\ 0 & 0 & \frac{35}{2}\alpha^3 & 56\alpha^3 \end{bmatrix}$$

$$C_{x3} = \begin{bmatrix} 0 & 0 & \frac{k_{44}\alpha\beta - 2(\alpha^2 - 1)}{144k_{44}} & \frac{2k_{44}\alpha^2 - 3k_{44}\alpha - \beta(3\alpha + 4)}{120k_{44}} \\ 0 & 0 & \frac{3k_{44}\alpha^2 - 2k_{44}\alpha - \beta(3\alpha + 4)}{120k_{44}} & \frac{k_{44}\alpha\beta - \alpha^2 + 1}{16k_{44}} \\ \frac{k_{44}\alpha\beta - 2(\alpha^2 - 1)}{144k_{44}} & \frac{3k_{44}\alpha^2 - 2k_{44}\alpha - \beta(3\alpha + 4)}{120k_{44}} & 0 & 0 \\ \frac{2k_{44}\alpha^2 - 3k_{44}\alpha - \beta(3\alpha + 4)}{120k_{44}} & \frac{k_{44}\alpha\beta - \alpha^2 + 1}{16k_{44}} & 0 & 0 \end{bmatrix}$$

in which  $\beta = \alpha - 1$ . Besides, we have the following relations:

$$\begin{cases} m_{x0} &= m_{x1} + f_{z1}u_{y1} - f_{y1}u_{z1} \\ m_{y0} &= m_{y1} - f_{z1} + f_{x1}u_{z1} \\ m_{z0} &= m_{z1} + f_{y1} - f_{x1}u_{y1} \end{cases} \quad (22)$$

These equations involve 15 parameters, including 6 deflection parameters and 6 load parameters at the free end, and 3 moments at the fixed end. Given any 6 parameters, the other 9 parameters can be obtained by simultaneously solving these equations using the Newton-Raphson method. The matrices in the model are dimensionless and valid for spatial beams of uniform and rectangular cross-section when deflected in the intermediate range. Similar to Ref. [27], matrix  $C_1$  represents the linear elastic compliances associated with the four transverse bending loads.  $C_2$  and  $C_4$  capture load stiffening effects in these directions in the presence of axial load  $f_{x1}$ . For example, in the presence of positive  $f_{x1}$ , because the first terms of  $C_2$  and  $C_4$  are negative, the total compliance in the  $u_y$  direction is reduced, which is the load stiffening effect.  $C_3$  and  $C_6$  capture load stiffening effects in the bending directions in the presence of torsional moment  $m_{x0}$  and reveal a resulting coupling between the two bending planes.  $C_5$  captures the coupling between the two bending planes in the presence of axial force  $f_{x1}$  and torsional moment  $m_{x0}$ . Although the matrix  $C_{t1}$  in Eq. (20) relates the torsional rotation to transverse direction loads, it can be shown that it captures the purely kinematic contributions of bending deflections to torsional rotation that was shown in Ref [27]. Similarly, the matrix  $C_{x1}$  in Eq. (21) captures the purely kinematic contribution of bending deflections to the axial deflection. In a similar manner,  $C_{t2}$  and  $C_{t3}$  in Eq. (20) and  $C_{x2}$  and  $C_{x3}$  in Eq. (21) capture the elastokinematic effects in axial direction and torsion direction, respectively.

As compared to SBCM that was developed for bisymmetric spatial beams, this model provides designers an analytical tool for modeling rectangular spatial beams. When  $\alpha = 1$  (i.e. the cross section of the beam is square), errors between these two load-displacement equations are less than 1%. Besides, there are two major differences between the load-displacement relations for these two models: (1) compliance terms are used in the rectangular beam's equations, while stiffness terms are used in the bisymmetric beam equations. Because the power series method does not provide closed-form load-displacement relations, it is hard to analytically transform the load-displacement equations (19) into a stiffness form. By setting  $\alpha = 1$  and numerically transforming this model to stiffness form with some simplification, we can find that there is just a little difference in the  $m_{x1}^2$  terms, which results in very small changes to the overall relations. (2) the load parameters at the free end are used in the bisymmetric spatial beam's equations, while the load parameters both at the fixed and the free ends take places in the rectangular beam's equations to make the load-displacement equations more compact in the modeling of rectangular beam.

### 5. Validation

This section provides validation of the end load-displacement equations (i.e. Eqs. (19)–(21)) using nonlinear finite element models (NLFEM) established in ANSYS and Abaqus. The flexible beam being analyzed is assumed to be made of steel with Young's modulus  $E = 2.1 \times 10^{11}$  Pa and Poisson's ratio  $\mu = 0.26$ . The length of the beam

$L = 0.2$  m, and the cross section is rectangular with width  $W = 0.006$  m and thickness  $T = 0.001$  m.

To guarantee the accuracy of the NLFEM results, the flexible beam was meshed into 50 elements using BEAM188 in ANSYS while 40 elements using B31 in Abaqus, respectively, with the geometric nonlinearities option turned on. It should be noted that the output tip angles in ANSYS and Abaqus are not clearly defined, and may be different from the Tait-Bryan angles used in this work (i.e.,  $\theta_{xd}$ ,  $\theta_{zd}$  and  $\theta_y$ ). For the purpose of comparison, a rigid structure consisting of three mutually perpendicular beams (AB, AC, and AD, as shown in Fig. 3) are introduced and attached to the tip of the beam (point A) in the NLFEM simulation to calculate the Tait-Bryan angles. Length of these three beams are 1. These structures can be considered as the deformed coordinate frame at the beam tip ( $X_{dL} - Y_{dL} - Z_{dL}$ ). The transformation matrix can be expressed by the coordinates of points A, B, C and D as:

$$R = \begin{bmatrix} r_{11} & r_{12} & r_{13} \\ r_{21} & r_{22} & r_{23} \\ r_{31} & r_{32} & r_{33} \end{bmatrix} = \begin{bmatrix} X_B - X_A & Y_B - Y_A & Z_B - Z_A \\ X_C - X_A & Y_C - Y_A & Z_C - Z_A \\ X_D - X_A & Y_D - Y_A & Z_D - Z_A \end{bmatrix} \quad (23)$$

With the transformation matrix in Eq. (1), the Tait-Bryan angles can be calculated by the following expressions

$$\begin{cases} \theta_{xd1} &= \arctan \frac{-r_{32}}{r_{22}} \\ \theta_{y1} &= \arctan \frac{-r_{13}}{r_{11}} \\ \theta_{zd1} &= \arctan \frac{r_{12}}{\sqrt{r_{11}^2 + r_{13}^2}} \end{cases} \quad (24)$$

The tip angles can be represented by the twisting angle ( $\theta_{xd1}$ ), the rotational angle in the  $XOZ$  plane ( $\theta_{y1}$ ) and the rotational angle in the  $XOY$  plane ( $\theta_{z1}$ ).  $\theta_{z1}$  can be derived by the Tait-Bryan angles as

$$\theta_{z1} = \arctan \frac{\tan \theta_{zd}}{\cos \theta_y} \quad (25)$$

Six load cases are employed to verify the correctness of the load-deflection equations, as listed in Table 1. For each load case, we guarantee that the deflections are within the intermediate range, that is, the normalized transverse deflections and the rotations won't exceed  $\pm 0.1$ .

For the first load case, Fig. 4 shows the variations of the normalized transverse deflections and the rotations of the beam as  $F_{yL}$  incrementally increases from  $-1$  N to  $1$  N in 21 load steps while other load parameters remain unchanged. The transverse deflections and the rotation angles obtained by this model agree well with those of the two commercial finite element software packages (ANSYS and Abaqus), except for the twisting angle  $\theta_{xd1}$ . Interestingly, the results of  $\theta_{xd1}$  obtained by ANSYS and Abaqus don't agree with each other, while this model's predictions fall in between those of the two software packages. To find out which one is more accurate, we simplified the load case to a pure torque load case ( $M_{xL} = 1$  and all other load parameters were set to 0). The corresponding results of  $\theta_{xd1}$  obtained by this model, ANSYS and Abaqus are 0.08045, 0.07742 and 0.08111, respectively. The torsion angle of this beam can be calculated analytically by using the infinite series expression of  $J$  [20]:

$$\Theta_x = \frac{M_x L}{GJ}$$

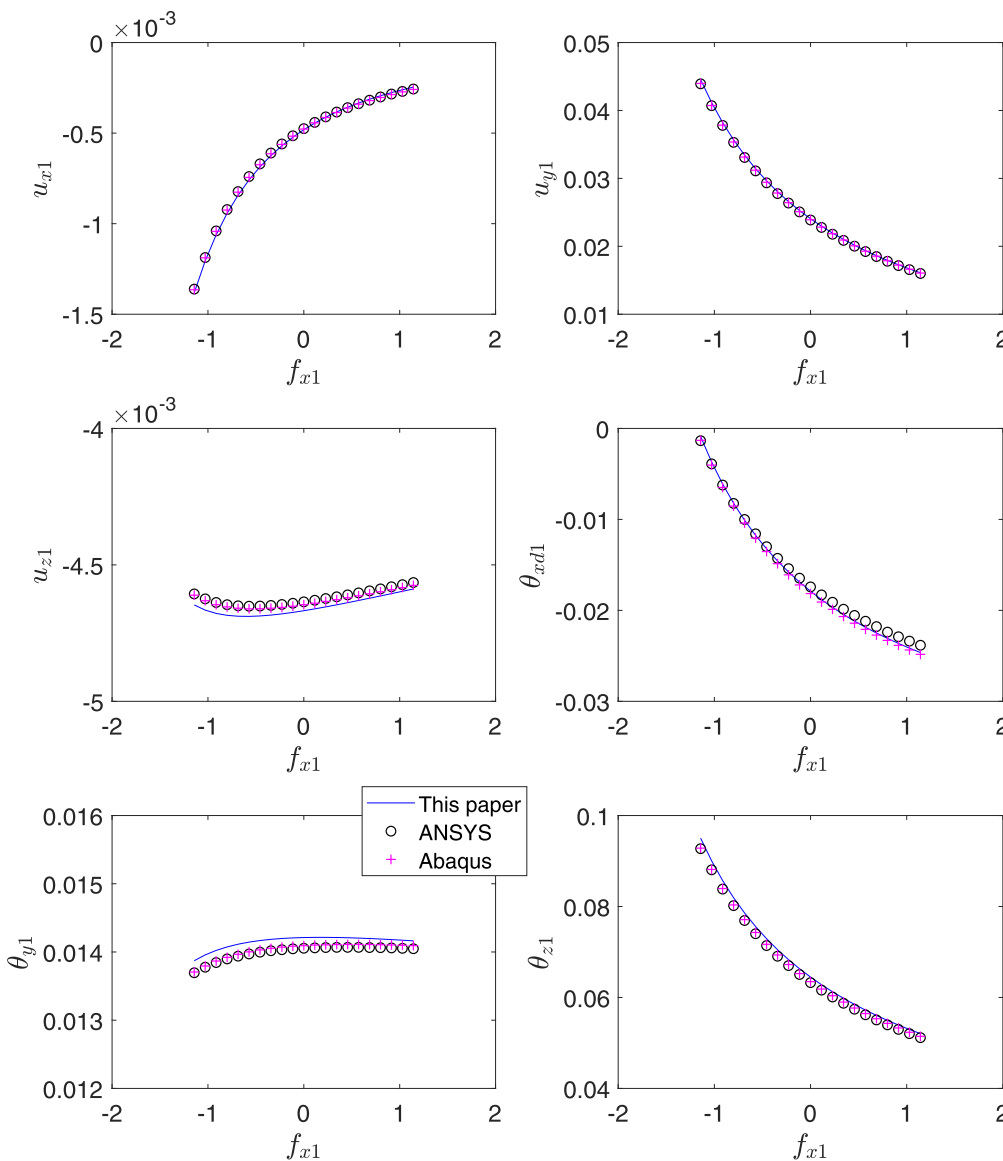


Fig. 8. Deflections vs.  $f_x$  (load case 5).

where

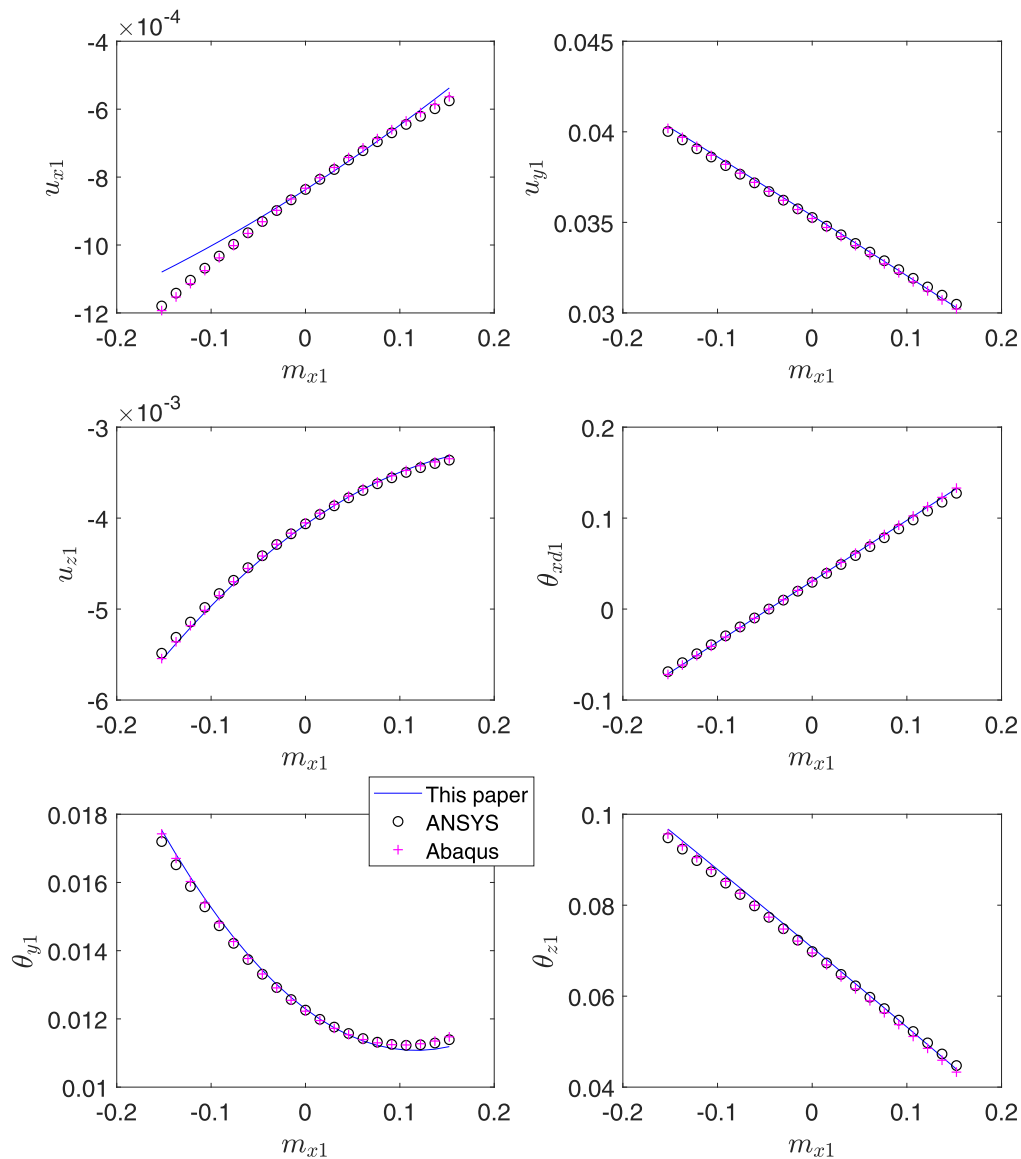
$$J = W^3 T \left( \frac{1}{3} - \frac{64}{\pi^5} \frac{W}{T} \sum_{i=1,3,5,\dots}^{\infty} \frac{\tanh(iT\pi/2W)}{i^5} \right)$$

and the analytical result is 0.08045. The results indicate that this model is more accurate in calculating the twisting angle, nevertheless, the errors between these methods are less than 5%. Similar results are observed in Fig. 5 for the second load case, in which  $M_{ZL}$  incrementally increases from  $-0.07 \text{ N}\cdot\text{m}$  to  $0.07 \text{ N}\cdot\text{m}$  in 21 load steps while other load parameters remain unchanged.

For the third and the fourth load cases, Figs. 6 and 7 show the variations of the normalized transverse deflections and the rotations of the beam with respect to varying  $F_{ZL}$  and  $M_{YL}$ , respectively. Again, the this models results for  $\theta_{xd1}$  fall in between those of ANSYS and Abaqus. This model and ANSYS agree well on predicting the axial elongation of the beam ( $u_{x1}$ ), while Abaqus yields relatively large errors (with the maximum error of 9%). For all the other transverse deflections and the rotation angles, the predictions of this model agree well with those of the two commercial finite element software packages.

At least 3 load parameters were set to 0 for each of the first 4 load cases. To demonstrate more general loading conditions for the spatial beam, we choose 5 non-zero load parameters and 1 varying load parameter for the fifth and the sixth load cases. Fig. 8 shows the results for the fifth load case, from which we can see that, the predictions of this model for all the transverse deflections and the rotation angles agree well with those of ANSYS and Abaqus. Although there are noticeable differences between this model’s predictions and those of ANSYS and Abaqus for  $u_{z1}$  and  $\theta_{y1}$  (corresponding to bending of the beam along the width direction), the relative errors are less than 1.3%. For the sixth load case, Fig. 9 shows that results of this model agree well with those of ANSYS and Abaqus except the axial elongation  $u_{x1}$ . The maximum prediction error of this model for  $u_{x1}$  is 8.3% and 9.3% as compared to ANSYS and Abaqus, respectively, which is still acceptable considering that  $u_{x1}$  is along the degree of constraint of the beam and is always very small.

Therefore, results of these load cases demonstrate that Eqs. (19)–(21) are precise enough to calculate the end-displacements when a general load exerts on the free end of the beam.

Fig. 9. Deflections vs.  $m_x$  (load case 6).

## 6. Conclusions

This paper has presented a compact nonlinear spatial beam that captures the constraint characteristics (i.e. stiffness and error motions) of a slender beam with a general rectangular cross-section via parametric end load-displacement relations that capture relevant geometric nonlinearities in spatial beam mechanics. Previous SBCM was limited to bisymmetric uniform cross-section slender beams. The new model is capable of capturing the relevant geometric nonlinearities in the intermediate deflection range (the transverse deflections and rotations are limited to  $0.1L$  and  $0.1$ , respectively) and offers a parameterized tool for understanding the constraint/motion behaviors of rectangular beams. The model was validated to be accurate by comparing to commercial finite element software packages. Our future work will be focused on extending this model for modeling large spatial deflections of rectangular beams by employing a discretization-based scheme. We also plan to validate the results of this paper via experimental testing.

## References

- [1] Awtar S, Sen S. A generalized constraint model for two-dimensional beam flexures: nonlinear load-displacement formulation. *ASME J Mech Des* 2010;132(8):081008.
- [2] Howell LL, Magleby SP, Olsen BM. *Handbook of compliant mechanisms*. John Wiley & Sons; 2013.
- [3] Chen G, Wilcox DL, Howell LL. Fully compliant double tensural tristable micromechanisms (dtm). *J Micromech Microeng* 2009;19(2):025011.
- [4] Chen G, Gou Y, Zhang A. Synthesis of compliant multistable mechanisms through use of a single bistable mechanism. *ASME J Mech Des* 2011;133(8):081007.
- [5] Liu Y, Xu Q. Design of a compliant constant force gripper mechanism based on buckled fixed-guided beam. In: *Manipulation, automation and robotics at small scales (MARSS), international conference on. IEEE*; 2016. p. 1–6.
- [6] Chen Y-H, Lan C-C. An adjustable constant-force mechanism for adaptive end-effector operations. *ASME J Mech Des* 2012;134(3):031005.
- [7] Chen G, Chang H, Li G. Design of constant-force compliant sarrus mechanism considering stiffness nonlinearity of compliant joints. In: *Advances in reconfigurable mechanisms and robots II*. Springer; 2016. p. 107–16.
- [8] Tolou N, Henneken VA, Herder JL. Statically balanced compliant micro mechanisms (sb-mems): concepts and simulation. In: *ASME 2010 international design engineering technical conferences and computers and information in engineering conference*. American Society of Mechanical Engineers; 2010. p. 447–54.
- [9] Chen G, Zhang S. Fully-compliant statically-balanced mechanisms without prestressing assembly: concepts and case studies. *Mech Sci* 2011;2(2):169–74.
- [10] Chen G, Ma F. Kinetostatic modeling of fully compliant bistable mechanisms using timoshenko beam constraint model. *ASMS J Mech Des* 2015;137(2):022301.
- [11] Ma F, Chen G. Bi-BCM: a closed-form solution for fixed-guided beams in compliant mechanisms. *ASME J Mech Rob* 2017;9(1):014501.
- [12] Howell LL, Midha A, Norton T. Evaluation of equivalent spring stiffness for use in a pseudo-rigid-body model of large-deflection compliant mechanisms. *ASME J Mech Des* 1996;118(1):126–31.

- [13] Campanile L, Hasse A. A simple and effective solution of the elastica problem. *Pro Inst MechEng Part C* 2008;222(12):2513–16.
- [14] Zhang A, Chen G. A comprehensive elliptic integral solution to the large deflection problems of thin beams in compliant mechanisms. *ASME J Mech Rob* 2013;5(2):021006.
- [15] Lai H-Y, Hsu J-C, et al. An innovative eigenvalue problem solver for free vibration of euler-bernoulli beam by using the adomian decomposition method. *Comput Math Appl* 2008;56(12):3204–20.
- [16] Saxena A, Kramer S. A simple and accurate method for determining large deflections in compliant mechanisms subjected to end forces and moments. *ASME J Mech Des* 1998;120(3):392–400.
- [17] Ma F, Chen G. Modeling large planar deflections of flexible beams in compliant mechanisms using chained beam-constraint-model. *ASME J Mech Rob* 2016;8(2):021018.
- [18] Kota S, Hetrick JA, Osborn R, Paul D, Pendleton E, Flick P, et al. Design and application of compliant mechanisms for morphing aircraft structures. In: *Smart structures and materials 2003: industrial and commercial applications of smart structures technologies*, 5054. International Society for Optics and Photonics; 2003. p. 24–34.
- [19] Awtar S, Trutna TT, Nielsen JM, Abani R, Geiger J. Flexdex™: a minimally invasive surgical tool with enhanced dexterity and intuitive control. *J Med Dev* 2010;4(3):035003.
- [20] Timoshenko S, Goodier J. *Theory of elasticity*. McGraw-Hill 1970;433.
- [21] Sen S. Beam constraint model: Generalized nonlinear closed-form modeling of beam flexures for flexure mechanism design.2013;
- [22] Chimento J, Lusk C, Alqasimi A. A 3-d pseudo-rigid body model for rectangular cantilever beams with an arbitrary force end-load. In: *ASME 2014 international design engineering technical conferences and computers and information in engineering conference*. American Society of Mechanical Engineers; 2014. V05AT08A029–V05AT08A029
- [23] Li G, Jia J, Chen G. Solving large-deflection problem of spatial beam with circular cross-section using an optimization-based runge-kutta method. *Int J Nonlinear SciNumer Simul* 2016;17(1):65–76.
- [24] Bathe K-J, Bolourchi S. Large displacement analysis of three-dimensional beam structures. *Int J Numer Methods Eng* 1979;14(7):961–86.
- [25] Hodges D.H., Dowell E.. *Nonlinear equations of motion for the elastic bending and torsion of twisted nonuniform rotor blades*1974;
- [26] Jonker JB, Meijaard JP. A geometrically non-linear formulation of a three-dimensional beam element for solving large deflection multibody system problems. *Int Non-Linear Mech* 2013;53:63–74.
- [27] Sen S, Awtar S. A closed-form nonlinear model for the constraint characteristics of symmetric spatial beams. *AMSE J Mech Des* 2013;135(3):031003.
- [28] Rasmussen NO, Wittwer JW, Todd RH, Howell LL, Magleby SP. A 3d pseudo-rigid-body model for large spatial deflections of rectangular cantilever beams. In: *ASME 2006 international design engineering technical conferences and computers and information in engineering conference*. American Society of Mechanical Engineers; 2006. p. 191–8.
- [29] Chase Jr RP, Todd RH, Howell LL, Magleby SP. A 3-d chain algorithm with pseudo-rigid-body model elements. *MechDesStructMach* 2011;39(1):142–56.
- [30] Hao G, Kong X, Reuben RL. A nonlinear analysis of spatial compliant parallel modules: multi-beam modules. *Mech Mach Theory* 2011;46(5):680–706.
- [31] Chen G, Bai R. Modeling large spatial deflections of slender bisymmetric beams in compliant mechanisms using chained spatial-beam constraint model. *ASME J Mech Rob* 2016;8(4):041011.
- [32] Nijenhuis M, Meijaard JP, Mariappan D, Herder JL, Brouwer DM, Awtar S. An analytical formulation for the lateral support stiffness of a spatial flexure strip. *ASME JMachDes* 2017;139(5):051401.
- [33] Ma F, Chen G. Chained beam-constraint-model (cbcm): a powerful tool for modeling large and complicated deflections of flexible beams in compliant mechanisms. In: *ASME 2014 international design engineering technical conferences and computers and information in engineering conference*. American Society of Mechanical Engineers; 2014. V05AT08A027–V05AT08A027
- [34] Chen G, Ma F, Hao G, Zhu W. Modeling large deflections of initially curved beams in compliant mechanisms using chained beam-constraint-model. *ASME J Mech Rob* 2018.
- [35] Chen G, Howell LL. Two general solutions of torsional compliance for variable rectangular cross-section hinges in compliant mechanisms. *PrecisEng* 2009;33(3):268–74.
- [36] Ince E. *Ordinary differential equations*, 1956; 1939.